Sub Topic: Laminar Flames Paper: 114LF-0452

9th U. S. National Combustion Meeting
Organized by the Central States Section of the Combustion Insitute
May 17-20, 2015
Cincinnati, Ohio

Ignition of *n*-Hexane-Air by Moving Hot Particles: Effect of Particle Diameter

*S. A. Coronel**, *J. Melguizo-Gavilanes and J. E. Shepherd*

Graduate Aerospace Laboratories, California Institute of Technology, Pasadena, California 91125, USA

* *Corresponding Author Email: coronel@caltech.edu*

Abstract: Hot particles represent a potential ignition hazard if they are ejected into flammable vapor. The present study aims at understanding the phenomenon of ignition by a single hot (inert) particle under well characterized conditions. This work investigates the ignition of *n*-hexane-air mixtures at a fixed equivalence ratio of 0.9 using alumina particles with diameters of 1.8 mm, 3.5 mm, and 6.0 mm moving with a velocity of approximately 2.4 m/s. The ignition threshold (i.e. minimum ignition temperature) was determined for each particle diameter. The experimental results reveal that the ignition threshold decreases as particle diameter increases. A 6.0 mm diameter particle has an ignition threshold of 980 K whereas a 1.8 mm diameter particle has a higher threshold of 1115 K. Numerical simulations of the ignition process yield similar trends when compared with experimental observations. ***Keywords: Hot Surface Ignition, Hexane, Minimum Ignition Temperature, Laminar Flames***

1 Introduction

Assessing the risk of accidental ignition of flammable mixtures is an issue of importance in industry and aviation. Of particular interest are the risks associated with the use of carbon fiber reinforced polymers (CFRP) as an alternative to aluminum alloys in aircraft manufacturing. Potential ignition sources in aircraft include: lightning strikes, sparks from electrical equipment, electrostatic discharge in fuel tanks, and overheated pumps. In the case of a lightning strike on the aircraft structure, hot particles are often ejected from the surface that is struck due to resistive heating. Such hot particles represent a potential ignition hazard if ejected into flammable vapor. The present study aims to contribute to the understanding of ignition by a single hot (inert) particle under well characterized conditions.

Previous experiments involving hot particle ignition include particles heated in a furnace and then shot into an explosive atmosphere, as well as stationary particles placed in an explosive atmosphere and heated via infrared laser light. The former experiment was performed by Silver [1] using two different particle materials, quartz and platinum. Varying the particle material had minimal effect on the minimum ignition temperature of three different flammable mixtures: a 10% coal-gas/air mixture, 3% pentane/air mixture, and a 20% hydrogen/air mixture. For a fixed gas mixture, his results suggest that the size and temperature of a particle are important factors in determining whether ignition occurs. The data indicate that as particle size is increased, the minimum temperature required for ignition decreases. The experiments performed by Silver were done with particle speeds varying from $2 - 5$

m/s; however, the effect of particle speed was not investigated systematically. More recently, Beyer and Markus [2] performed studies using inert particles suspended in an explosive atmosphere and heated via infrared laser light. The combustible mixtures used in [2] were pentane/air, propane/air, ethylene/air and hydrogen/air. Their studies showed that the particle ignition temperature was weakly dependent on the mixture composition but significantly more sensitive to the combustible gas used. The particle ignition temperature was also highly dependent on the particle diameter. Roth et. al [3] studied the ignition of hydrogen/air mixtures by submillimeter-sized particles and determined that the particle material (silicon nitride, tungsten carbide, steel, casting steel, and aluminum) had an effect on the ignition temperature for a fixed mixture composition. Their results suggest that chemically inert particles show the lowest surface temperature required for ignition when compared to the metal particles. Additional work on stationary hot particle ignition via laser light has been performed by Dubaniewicz et. al [4, 5], Dubaniewicz [6], Bothe et al. [7], Beyrau et al. [8], and Homan [9]. A comparison of the experimental data of Beyer and Markus, and Silver, for a pentane/air mixture shows that, when the diameter is kept fixed, a moving particle will have a higher ignition temperature than a stationary particle. Having reviewed these previous experiments, it is our view that existing work on moving hot particles in a flammable mixture is limited and deserves further study.

The aim of this work is to investigate the ignition of *n*-hexane-air mixtures, a simple surrogate for kerosene, using moving hot particles. Tests are performed using alumina particles with diameters varying from 1.8 mm to 6 mm at a fixed mixture composition ($\Phi = 0.9$) and with varying particle surface temperatures. Our study focuses on inert particles to minimize the complexity of the problem.

2 Experimental Setup

The ignition experiments were performed in a closed, cylindrical, stainless steel combustion vessel with a volume of approximately 22 L, shown in Fig. 1. Two parallel flanges are used to mount windows for visualization. Above the vessel, sits a cylindrical aluminum chamber with a volume of approximately 0.1 L, also shown in Fig. 1. The aluminum chamber is used to contain the heated spheres. It has two parallel flanges that are used to mount titanium supports, one of which can be actuated linearly through a double acting pneumatic actuator. To heat a sphere, the titanium supports make contact with the sphere on opposite sides holding it in place. The spheres are irradiated on opposite sides with a continuous-wave (cw) CO_2 laser (Synrad), shown in Fig. 2, that has a maximum power output of 80 W with an emission wavelength of 10.6 μm. The temperature of the sphere surface is measured using a two-color pyrometer.

Once a sphere is in place, a remotely controlled plumbing system is used to evacuate the combustion vessel and accurately fill it with the reactive mixture using the method of partial pressures, shown in Fig 1(a). A Heise manometer with a precise digital readout measures the static pressure so the gases can be filled to within 0.01 kPa of the desired gas pressure, providing precise control over the mixture composition. The aluminum chamber and attached cylinder, shown in Fig. 1(b), are filled with nitrogen through a port on the chamber. The bottom end of the cylinder has an electric optical shutter that is closed once the chamber and cylinder are completely filled with nitrogen. This ensures that during heating, the sphere is in an inert environment and there is minimal diffusion of the nitrogen from the chamber into the reactive mixture. The bottom end of the cylinder is vertically aligned with the top of the combustion vessel windows. A PID controller interfaces with the laser controller thereby allowing precise control of the sphere surface temperature during heating. Once the desired sphere surface temperature is reached, one of the titanium supports retracts allowing the sphere to fall, shown

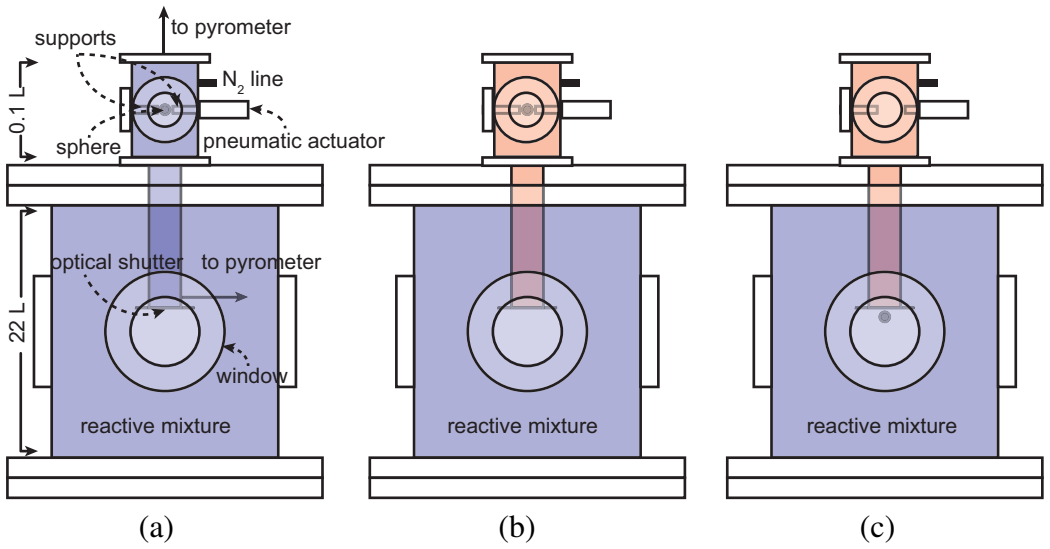

Figure 1: Experimental procedure for igniting a reactive mixture using a moving hot sphere, reactive mixture is shown in blue and N_2 is shown in red

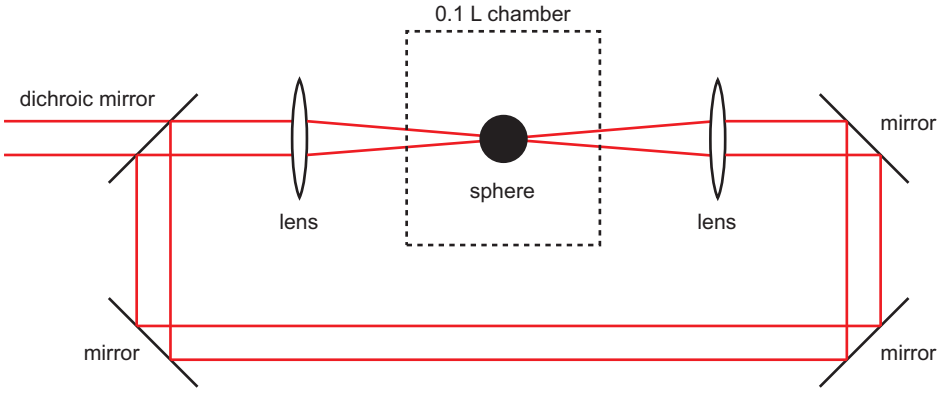

Figure 2: Beam splitting of CO_2 laser beam, shown in red; lenses are used to vary the beam spot size on the sphere surface

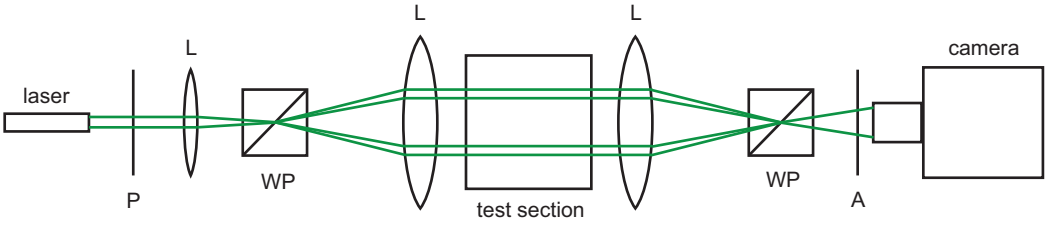

Figure 3: Shearing interferometer schematic (P: polarizer, L: lens, WP: Wollaston prism, A: analyzer)

in Fig. 1(c). The sphere travels through the cylinder (containing nitrogen) and then exits through the now open optical shutter into the combustion vessel (containing the reactive mixture) and comes into the field of view of the windows. The pyrometer measures the sphere surface temperature during heating and it is recorded prior to entering the reactive mixture as indicated in Fig. 1(a). Four different methods were used for ignition detection. First, the pressure rise from the combustion was measured using a pressure transducer. This measurement also allowed us to determine the peak pressure rise in the vessel. Second, the temperature rise was detected using a K-type thermocouple located inside the vessel. Third, the rise in signal from the two-color pyrometer photodetectors corresponding to the flame emission. The fourth method was a shearing interferometer, the optical setup is shown in Fig. 3. The shearing interferometer uses Wollaston prisms and a Coherent Sapphire 532 nm single mode laser to visualize the ignition and flame propagation using a high-speed camera at $10,000$ frames per second and a field of view of approximately 30 mm.

3 Phase Demodulation

The interferograms obtained with the shearing interferometer represent the optical path length difference between light that travels through a field of view with refractivity $n(z)$ and light that travels through a reference field with refractivity $n_0(z)$. The difference in phase, $\Delta\varphi$, is related to the index of refraction by,

$$\Delta\varphi = \varphi - \varphi_0 = \frac{2\pi}{\lambda}\int_{\zeta_1}^{\zeta_2}[n(z) - n_0(z)]dz, \tag{1}$$

where ζ_1 and ζ_2 are the locations along the $z-$axis where a ray enters and leaves the test section, respectively, and λ is the wavelength of the light in a vacuum. In the current study, $\lambda = 5.32 \times 10^{-7}$ m. The intensity, I, of a two-dimensional fringe pattern can be represented by an amplitude and frequency modulated function,

$$I\left(x,y\right) = a\left(x,y\right) + b\left(x,y\right)cos\left(\varphi\left(x,y\right)\right), \tag{2}$$

where a represents the background illumination and noise, b is the constrast variation, and φ is the phase [10]. The phase demodulation of the interferograms, i.e. obtaining φ, can be accomplished by using the Windowed Fourier Ridges (WFR) method which is described in [11]. If the index of refraction is cylindrically symmetric, as indicated in Fig. 4, the Abel transform, Eq. 3, can be used to transform Eq. 1 to cylindrical coordinates.

$$F(x) = 2\int_x^\infty \frac{f(r)r}{(r^2 - x^2)^{1/2}}dr. \tag{3}$$

The inverse Abel transform is given by

$$f(r) = -\frac{1}{\pi}\int_r^\infty \frac{dF}{dx}\frac{dx}{(x^2 - r^2)^{1/2}}, \tag{4}$$

where in the context of refractive index and optical phase difference,

$$f(r) = \frac{2\pi}{\lambda}[n(r) - n_o(r)] \quad \text{and} \quad F(x) = \Delta\varphi \tag{5}$$

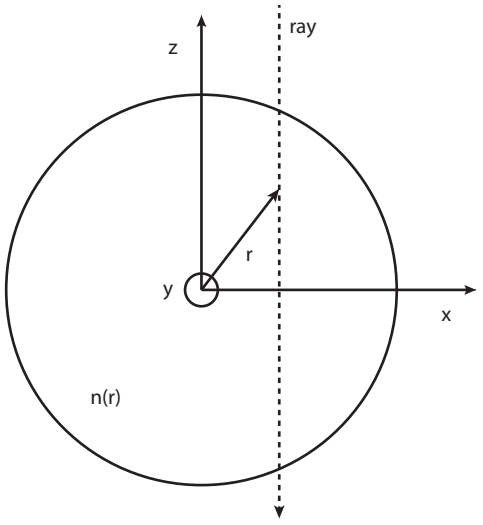

Figure 4: Light wave passing through a radially symmetric medium

The density of the medium can then be found through the Gladstone-Dale relation, Eq. 6, where $K = 2.274 \times 10^{-4}$ m^3/kg at room temperature and pressure [12].

$$n - 1 = K\rho, \tag{6}$$

The refractive index is dependent on the composition of the medium, the temperature and pressure of the medium and the wavelength of the light source used. For ideal gases at constant pressure, Eq.6 can be given by

$$n - 1 \propto 1/T. \tag{7}$$

therefore,

$$\frac{n-1}{n_0-1} = \frac{T_0}{T}, \tag{8}$$

where T_0 is the reference field temperature. If δ is defined as $n - 1$, then

$$\frac{\delta}{\delta_0} = \frac{T_0}{T}. \tag{9}$$

For air at room temperature and pressure, $\delta_0 = 2.93 \times 10^{-4}$, therefore, the variation of δ with temperature is given in Fig. 5. At lower temperatures, a change in temperature yields a large change in δ, however at higher temperatures, the changes in δ become smaller. Changes in the refractive index will clearly be observed following an ignition and flame propagation of a flammable mixture in which the temperature of the gas will range from 300 K (fresh reactants) to approximately 2000 K (adiabatic flame temperature) [13]. In terms of the composition, the refractive index of the medium (i.e. igniting flammable mixture followed by a flame propagation) changes due to bond rearangements and volume

changes due to the change in the number of moles. However, Weinberg [14] determined that in combustion processes, the change in refractive index due to composition changes are small compared to changes due to temperature; changes due to bond rearrangements are even smaller.

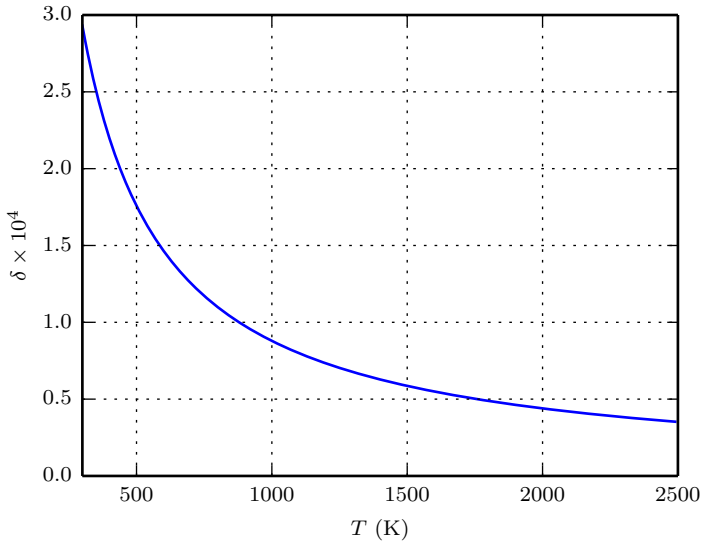

Figure 5: δ **vs.** T

To demontrate the small change in δ due to the change in number of moles, consider the stoichiometric oxidation in air of *n*-hexane (C_6H_{14}),

$$\begin{gathered} C_6H_{14} + 45.2(0.21O_2 + 0.79N_2) \longrightarrow 6CO_2 + 7H_2O + 35.7N_2 \\ \delta_{reactants} = (\delta_{C_6H_{14}} + 9.5\delta_{O_2} + 35.7\delta_{N_2})/46.2 = 0.000329 \\ \delta_{products} = (6\delta_{CO_2} + 7\delta_{H_2O} + 35.7\delta_{N_2})/48.7 = 0.000311. \end{gathered}$$

The change in δ due to the change in number of moles is approximately 5%.

4 Numerical approach and simulation parameters

4.1 Overview

We model the heat transfer and ignition process by the numerical simulation of the variable-density reactive Navier-Stokes equations with temperature dependent transport properties. The governing equations are integrated in two dimensions using the Open source Field Operation And Manipulation (OpenFOAM) toolbox [15]. The Sutherland Law, the Eucken Relation and the JANAF polynomials are used to account for the functional dependence of mixture viscosity, thermal conductivity and specific heat at constant pressure respectively. The ratio of thermal to mass diffusivity is assumed to be unity ($Le = 1$). The spatial discretization of the solution domain is done using finite volumes, and the pressure-velocity coupling is achieved using the PIMPLE (PISO+SIMPLE) algorithm. The computational domain consists of a square of side $20d$, with a "sphere" (cylinder in 2D) diameter, d, of 2.0, 4.0, 6.0, and 8.0 mm located in the center. A resolution of approximately 300000 cells is

used, with finer resolution near the sphere, using a minimum cell size of 60 μm to ensure that the thermal/hydrodynamic boundary layers are properly resolved. The simulation is carried out with initial and boundary conditions that reproduce the experimental conditions described in section 3. The numerical integration is divided in two parts: first, a free fall in N_2 for 250 ms (fall time measured experimentally) during which a steady thermal boundary layer develops. Second, contact with a slightly lean *n*-hexane-air mixture ($\Phi = 0.9$) for 20 ms (experimental observation window). The simulation is stopped if ignition does not occurs within the experimental observation window. The chemistry is modeled using an irreversible one-step scheme ($R \rightarrow P$) in which the kinetic parameters are fitted to match the ignition delay times of the updated Ramirez detailed mechanism [16] at an initial pressure, P_0, of 101 kPa for gas temperatures of $900 - 1600$ K. The simulation initial conditions are: $P_o = 101$ kPa, $T_0 = 300$ K, $\mathbf{U}_o = (\, u_0 \,, v_0 \,, w_0 \,)$ m/s where $u_0 = v_0 = w_0 = 0$, and a constant sphere surface temperature. The frame of reference is attached to the sphere, hence, a time dependent inflow boundary condition is prescribed at the bottom of the computational domain to properly simulate the fall of the heated particle, given by $\mathbf{U}(t) = (\, 0 \,, gt \,, 0 \,)$ m/s. At the top, a non-reflective/pressure transmissive boundary condition is used to simulate an outflow.

4.2 Validation

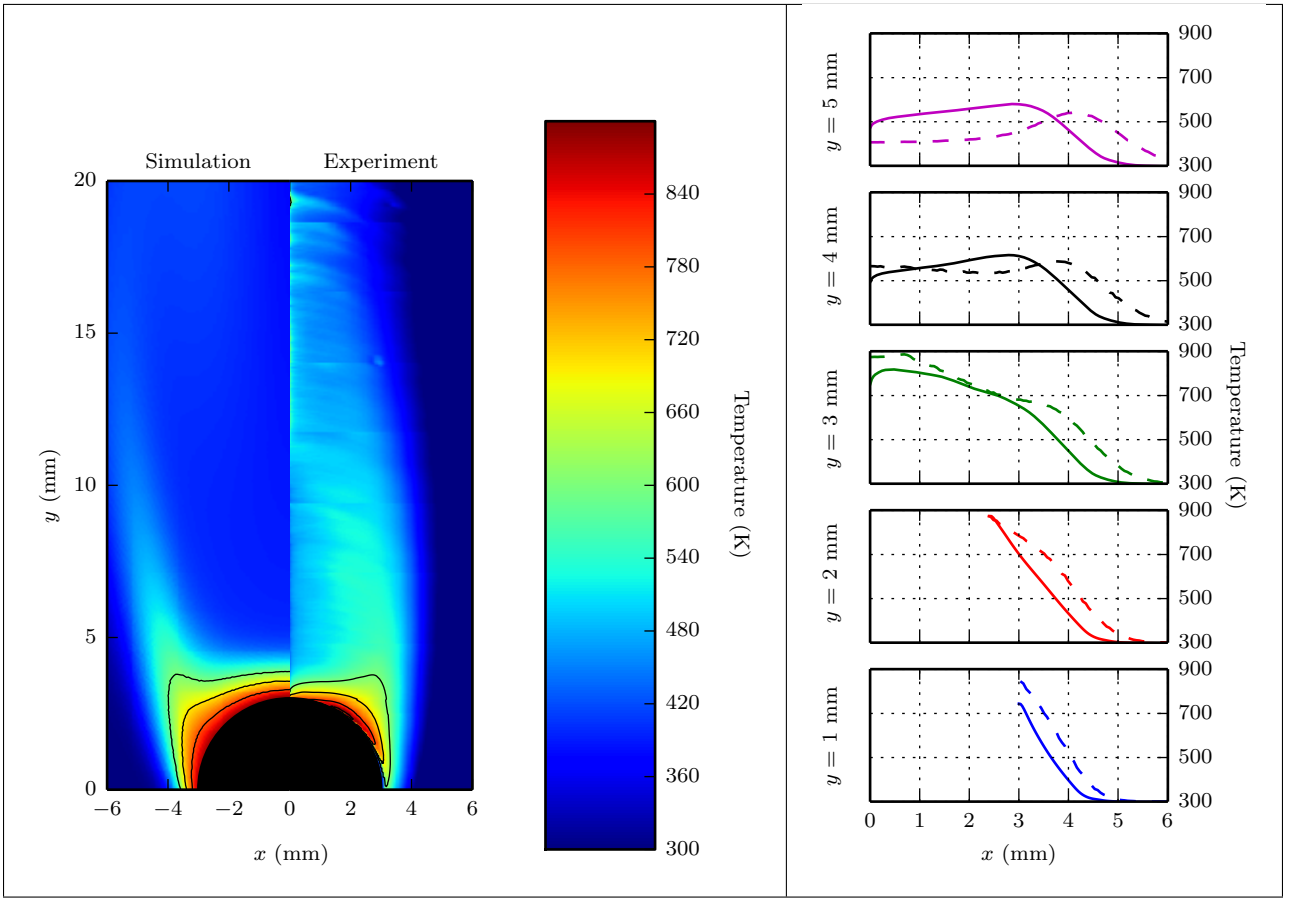

Figure 6: (Left) Gas (air) temperature with contour lines of constant temperature: simulation (left) and experiment (right); (Right) temperature along slices of y, simulation:– – – and experiment:———

An experimental temperature field of air heated by a 6.0 mm diameter sphere was compared with a simulated temperature field to validate the numerical results. Figure 6 (left) shows the temperature field and contour lines of constant gas temperature obtained experimentally and numerically. The simulation predicts a smaller temperature gradient in the rear stagnation point of the sphere when compared to the experiment. In both the experiment and simulation, the temperature gradient decreases along the curvature of the sphere. The region of flow separation is where the maximum thermal boundary layer thickness is observed. The wake appears wider in the simulation, however, this is because a cylinder rather than a sphere is simulated. Figure 6 (right) shows the gas temperature along slices of y (axial direction). The trends observed are very similar between the experiment and simulation in the region of interest, namely, up to the flow separation ($y \approx 2$ mm), where ignition is predicted to occur when close to the ignition threshold. The differences between the experiment and simulation can be attributed to the limitations of the phase demodulation near boundaries (i.e. near the sphere surface), the modeling of a cylinder rather than a sphere, and error introduced when calculating the derivative in the inverse Abel transform.

5 Results

5.1 Overview

Ignition tests were carried out for *n*-hexane-air mixtures at an initial temperature and pressure of 298 K and 100 kPa, respectively. The mixture equivalence ratio, Φ, was fixed at 0.9 and alumina spheres 1.8 mm, 3.5 mm and 6.0 mm in diameter were used as the ignition source. A sphere reaches the field of view approximately 200 ms after being dropped, during that time, each one has accelerated to approximately 2.4 m/s. Figure 7 shows interferograms of a no ignition event and an ignition event taken at similar times from 1 ms to 13 ms using a 6.0 mm diameter sphere. Each interferogram shows contours of constant index of refraction integrated through the field of view. The flow field is axisymmetric, about the path of the particle motion in most cases, so that Eq. 4 can be used to determine the radial distribution of the index of refraction from the images. The outer contour surrounding each sphere is analogous to the edge of the thermal boundary layer. The thin fringes represent regions in which a large temperature gradient is present, and the thicker fringes represent smaller temperature gradients. The no ignition images show that the temperature gradient is largest at the front stagnation point (as indicated by the thin fringes), and decreases (as indicated by the increase in thickness of the fringes) with increasing thermal boundary layer thickness along the streamwise direction until the flow separates. The flow appears steady and axisymmetric; the wake is composed of a steady toroidal vortex for Reynolds numbers, Re, between 20 and 210 in uniform temperature flows, as discussed by Johnson and Patel [17]. In the current study the Reynolds number is not uniquely defined due to the strong variation of the fluid properties through the boundary layer and wake region. Using the hot flow properties of the conditions tested, $Re = 335 - 409$, $Re = 193 - 206$, and $Re = 92 - 113$ for the 6.0 mm, 3.5 mm, and 1.8 mm diameter spheres, respectively. Flows with $Re = 335 - 409$ are not axisymmetric but will appear as such depending on the plane that is being viewed [17]. In the ignition case of Fig. 7, the flow around the sphere remains similar to the no ignition case up to 3.5 ms, after that time, the fringes begin to expand outwards away from the wake of the sphere indicating that ignition has taken place.

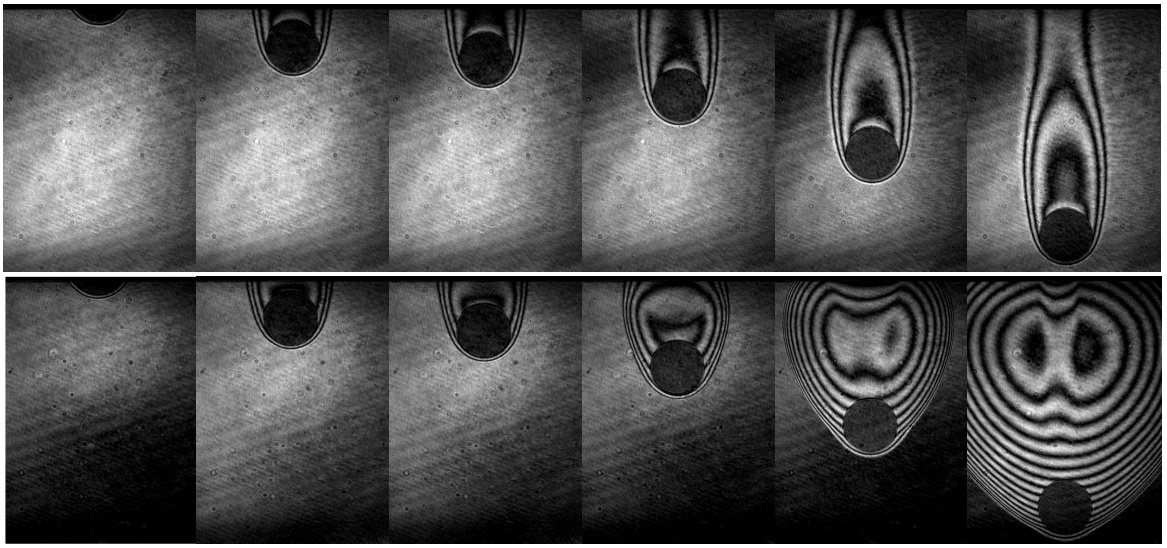

$t = 1.0$ ms $t = 3.5$ ms $t = 4.1$ ms $t = 5.9$ ms $t = 8.7$ ms $t = 12.6$ ms

Figure 7: Infinite fringe interferometer images of a no ignition (top) and ignition (bottom) events with sphere temperatures of 979 ± 27 K and 981 ± 1 K , respectively, in *n*-hexane-air with an equivalence ratio of 0.9

5.2 Ignition Threshold

The sphere surface temperature was varied from approximately 790 K to 1200 K; ignition and no ignition events are shown in Fig. 8 along with the ignition thresholds obtained numerically. Experimentally, the ignition threshold was found to be 981 ± 10 K, 1010 ± 25 K, and 1159 ± 10 K, for sphere diameters of 6.0 mm, 3.5 mm and 1.8 mm, respectively. Previous work done by Boettcher [18] using a stationary glow plug to ignite an *n*-hexane-air mixture at $\Phi = 0.9$ found an ignition threshold of $910 + 110/-0$ K using a glowplug 9.3 mm in height and 5.1 mm in diameter, this is approximately 7% lower than the threshold found in the current study for a 6.0 mm diameter sphere.

The simulation ignition thresholds are approximately 400 K higher than the experimental results. This large difference is attributed to uncertainties in the reaction mechanism used to obtain the one-step model as well as the differences between the geometry of the simulation and experiments. A preliminary conclusion is that the ignition behavior of hydrocarbons in the temperature range where ignition is observed experimentally is too complex to be predicted by a simple one-step model. There is a similarity in the experimental and simulation trends: as the diameter decreases, the ignition temperature increases. Silver [1] observed a small temperature gradient for sphere diameters of 5.5 mm using pentane/air, coal-gas/air and hydrogen/air mixtures and an increasing gradient with decreasing sphere diameter. The simulation predicts temperature differences similar to those observed experimentally. The experimental ΔT between 6.0 mm and 1.8 mm is < 150 K, the simulation ΔT between 6.0 mm and 2.0 mm is 100 K.

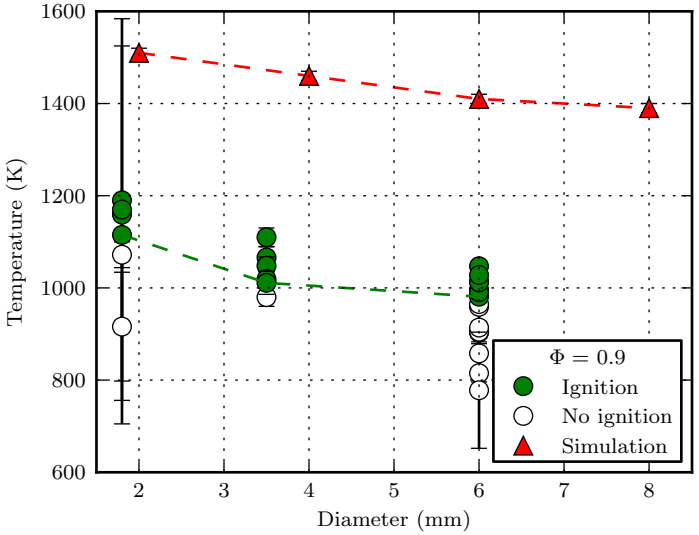

Figure 8: Hot particle ignition temperature as a function of sphere diameter at atmospheric temperature and pressure

5.3 Flame Propagation

Figure 9 shows flame propagations away, which appear axisymmetric, from three different sphere diameters. The time indicated below each set of images corresponds to the time elapsed from the sphere entering the field of view. According to the flame emission observed by the two-color pyrometer, Fig. 9(a) and (b) ignited 4.2 ms and 2.6 ms, respectively, pior to entering the field of view and Fig. 9(c) ignited 3.2 ms after entering the field of view. At $\Phi = 0.9$, the flame has a propagation speed of approximately 2.6 m/s [19] which is comparable to the sphere speed of 2.4 m/s. Figure 9 shows flames that propagate outwards except near the front stagnation point where it remains anchored to each sphere. The flame geometry and flame/sphere interaction suggests that the sphere speed is larger than the flame propagation speed. From the interferograms, it also appears that the flame anchoring is independent of the sphere diameters tested and only depends on the mixture composition. Experiments, not included in the current study, carried out in a stoichiometric mixture have higher flame speeds that result in the flame propagating away from the front stagnation point of the sphere. A mixture with 60% N_2 had a flame propagation speed and order of magnitude higher than the sphere speed which resulted in a flame that had a nearly spherical shape, similar to that found with a point source, and was not influenced by the presence of the sphere.

Figure 10 shows interferograms taken for each sphere diameter 8 ms after ignition. The figure shows the measured flame angle relative to the horizontal at the centerline of the sphere, indicated by the orange dashed lines. The measured flame angle is 73°, 71°, and 69° for the 6.0 mm, 3.5 mm, and 1.8 mm diameter spheres, respectively. The flame angle, as defined in Fig. 10, decreases as the flame propagates in time; this is observed in Fig. 9 for all three sphere diameters.

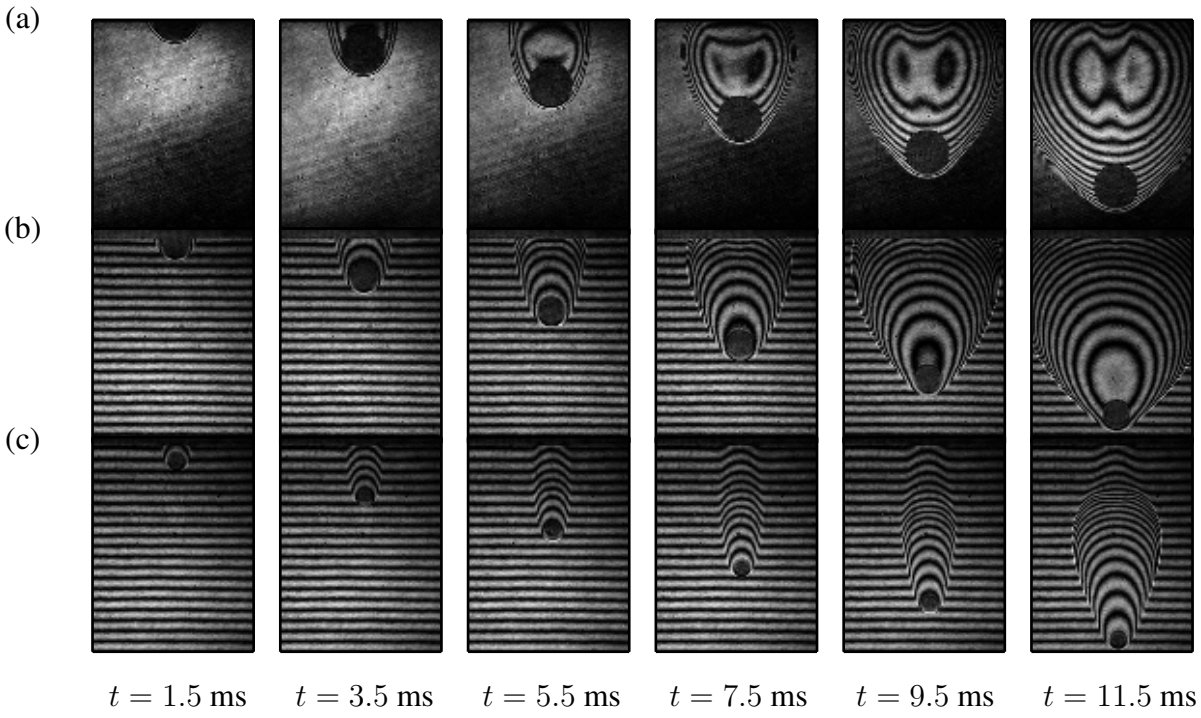

Figure 9: Interferograms of ignition and flame propagation for (a) 6.0 mm, (b) 3.5 mm, and (c) 1.8 mm diameter spheres

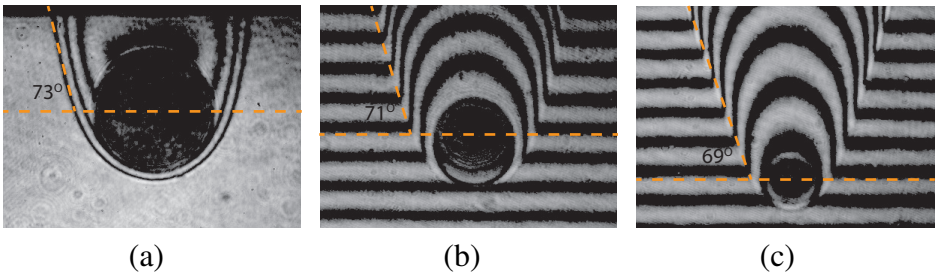

Figure 10: Interferograms 8 ms after ignition for (a) 6.0 mm, (b) 3.5 mm, and (c) 1.8 mm diameter spheres

6 Conclusions

In the present study, the ignition of *n*-hexane-air mixtures by moving hot spheres has been experimentally investigated for a range of sphere diameters at a fixed mixture composition of $\Phi = 0.9$. The ignition threshold was found to be 981 K $\pm$ 10 K, 1010 K $\pm$ 25 K, and 1159 K $\pm$ 10 K, for sphere diameters of 6.0 mm, 3.5 mm and 1.8 mm, respectively. Smaller diameters (< 1.8 mm) should be tested to observe a larger gradient in the ignition temperature. Simulations with a cylindrical geometry predicted an ignition temperature 400 K higher than the experimental thresholds, however, a similar trend and temperature difference between different particle sizes were observed. The interferograms showed that the flame remains anchored to the front stagnation point. This is expected for the mixture composition tested since the sphere and flame speeds are of comparable magnitude.

7 Acknowledgements

This work was carried out in the Explosion Dynamics Laboratory of the California Institute of Technology, S. A. Coronel was supported by The Boeing Company through a Strategic Research and Development Relationship Agreement CT-BA-GTA-1 and J. Melguizo-Gavilanes by the Natural Sciences and Engineering Research Council of Canada (NSERC) Postdoctoral Fellowship Program.

References

[1] R. S. Silver. *The London, Edinburgh, and Dublin Philosophical Magazine and Journal of Science*, 23 (1937) 633–657.

[2] M. Beyer and D. Markus. *Sci. Tech. Energetic Materials*, (2012) journal.

[3] David Roth, Pratyush Sharma, Thomas Haeber, Robert Schiessl, Henning Bockhorn, and Ulrich Maas. *Combustion Science and Technology*, 186 (2014) 1606–1617.

[4] Thomas H Dubaniewicz, Kenneth L Cashdollar, Gregory M Green, and Robert F Chaiken. *Journal of Loss Prevention in the Process Industries*, 13 (2000) 349 – 359.

[5] Thomas H. Dubaniewicz, Kenneth L. Cashdollar, and Gregory M. Green. *Journal of Laser Applications*, 15 (2003) 184–191.

[6] Thomas H. Dubaniewicz. *Journal of Laser Applications*, 18 (2006) 312–319.

[7] H. Bothe, S. Schenk, S. Hawksworth, F.B. Carleton, and F.J. Weinberg. The safe use of optics in potentially explosive atmospheres. In *Explosion Safety in Hazardous Areas, 1999. International Conference on (Conf. Publ. No. 469)*, pages 44–49, 1999.

[8] F. Beyrau, M. A. Hadjipanayis, and R. P. Lindstedt. *Proceedings of the Combustion Institute*, 34 (2013) 2065–2072.

[9] H. S. Homan. *Proceedings of Eighteenth Symposium (International) on Combustion*, (1981) 1709–1717.

[10] P. Rastogi and E. Hack, editors. *Phase Estimation in Optical Interferometry*. CRC Press, 2015.

[11] Qian Kemao. *Appl. Opt.*, 43 (2004) 2695–2702.

[12] W. Merzkirch. *Flow Visualization*. Academic Press, 1987.

[13] Chung K. Law. *Combustion Physics*. Cambridge University Press, 2006. Cambridge Books Online.

[14] F. J. Weinberg. *Optics of Flames*. Butterworth and Co. (Publishers) Ltd., 1963.

[15] H. G. Weller, G. Tabor, H. Jasak, and C. Fureby. *Comput. Phys.*, 12 (1998) 620–631.

[16] H.P. Ramirez, K. Hadj-Ali, P. Diévart, G. Dayma, C. Togbé, G. Moréac, and P. Dagaut. *Proceedings of the Combustion Institute*, 33 (2011) 375 – 382.

[17] T. A. Johnson and V. C. Patel. *Journal of Fluid Mechanics*, 378 (1999) 19–70.

[18] P. A. Boettcher. *Thermal Ignition*. PhD thesis, California Institute of Technology, 2012.

[19] S. A. Coronel, R. Mével, P. Vervish, P. A. Boettcher, V. Thomas, N. Chaumeix, N. Darabiha, and J. E. Shepherd. Laminar burning speed of n-hexane-air mixtures. In *8th US Combustion Meeting*, 2013.